NANO LETTERS

2005
Vol. 5, No. 10
2063−2069

Bioconjugated Superstructures of CdTe Nanowires and Nanoparticles: Multistep Cascade Förster Resonance Energy Transfer and Energy Channeling

Jaebeom Lee,[†] Alexander O. Govorov,[‡] and Nicholas A. Kotov*,[†]

Department of Chemical Engineering, Biomedical Engineering, and Material Sciences and Engineering, University of Michigan, Ann Arbor, Michigan 48109, and Department of Physics and Astronomy, Ohio University, Athens, Ohio 45701

Received June 4, 2005; Revised Manuscript Received August 18, 2005

ABSTRACT

Nanoparticle/nanowire assemblies with a degree of radial organization were prepared around luminescent semiconducting CdTe nanowires using bioconjugation with streptavidin and D-biotin linkers. Red-emitting nanowires (6.62 ± 1.55 nm diameter, 512 ± 119 nm length) and green-emitting nanoparticles (3.2 ± 0.7 nm diameter) were surface-modified with biotin, while orange-emitting nanoparticles (4.1 ± 1.2 nm diameter) were decorated with streptavidin. CdTe nanocrystals produced two fuzzy layers around the nanowires in which the diameter of CdTe nanoparticles decreased with the distance from the nanowire axis. Förster resonance energy transfer (FRET) from the outside layer of nanoparticles to the central nanowire was observed for nanowires conjugated with 4.1 nm CdTe. Addition of 3.2 nm CdTe resulted in a red–orange–green optical progression with band gaps of CdTe decreasing toward the axis of the superstructure. In this case, 4-fold luminescence enhancement of the nanowire luminescence was observed and was attributed to multistep FRET. This observation indicated the accumulation of photogenerated excitons in the cascade terminal. A simple model of multiconjugated superstructure with cascade energy transfer is developed and used to describe and understand the experimental data. The experimental data and theoretical model suggest the possibility of utilization of the prepared superstructures with radial symmetry in several classes of optoelectronic devices including nanomaterials for energy collection. They can also be a convenient model object for the investigation of methods of energy funneling in nanoscale assemblies.

Introduction. Rearrangement of nanoscale building blocks is a new research field focused on preparation of nanoscale superstructures and understanding the fundamental rules of their organization from an assortment of available structural nanoscale elements. Its practical importance is typically associated with a variety of electronic and photonic devices that can be built from nanocolloids by a simple technique of self-organization, although these may not be the only two areas where such systems will find interesting applications. A certain analogy can be drawn between nanoscale superstructures and widely investigated supermolecular systems sharing similar building block approach but with the difference in the nature of structural elements. A high degree of structural complexity can be obtained in molecular superstructures made from metal complexes.[1−5] They were particularly popular for mimicking photosynthetic organs of plants and bacteria.[6−8] In fact, some of them included porous films from TiO_2 nanoparticles.[9−11] Besides continued research in solar energy conversion, the same principle of nanoscale organization can be extended now in the design of molecular electronic devices.[12]

The dominant bonds that made possible assembly of supermolecules remain direct covalent bonding[13−15] and metal complexation.[16] When superstructures of similar complexity are to be built from nanoscale building blocks, a different approach needs to be found because of the intrinsic difference in scales between the bond length and the characteristic size of the assembly. In the past, our research group tested the possibility of the preparation of nanoparticle analogues of supramolecules with metal complexes as linkers[17] but found that they are unstable.[18] At least, two approaches can be used to solve this problem. First one is to learn more about structural anisotropy of nanoparticles and other building blocks that can increase specificity of their interactions. Substantial advances have been made in this direction recently.[13,14,19,20] Development of better understanding of anisotropic interactions between NPs constitutes a significant portion of research done in our group and will be reported separately. The second approach is to take advantage of the biological linkers such as DNAs and proteins, for which the length of the "bond" they create due to manifold of noncovalent interactions is comparable to the

* Corresponding author: kotov@umich.edu.
[†] University of Michigan.
[‡] Ohio University.

10.1021/nl051042u CCC: $30.25
Published on Web 09/23/2005

dimensions of the nanoscale building blocks. Additional advantage of proteins as linkers can be their specificity, versatility, and multivalent nature that can be imparted to the mutual interactions of nanoscale building blocks. Their biological functionality, such as antigen, antibody, signal membrane proteins, host−guest molecules, and many others,[21−24] are also of interest because they can lead to various biomedical applications of nanocolloids.

In this paper, we demonstrate superstructures from nanowires (NWs) and nanoparticles (NPs) with a degree of radial organization. The biotin−streptavidin pair was used to link different building blocks together. The assembly does not have spatial exactness typical for covalent bonds and can be characterized as a fuzzy superstructure. Similarly to many layer-by-layer (LBL) assembled polyelectrolyte multilayers,[25,26] this feature can actually be very beneficial for their functional properties and bring them closer to living biological systems. Here we demonstrate that one can obtain in the NW−NP superstructures an interesting and probably the first case of multistep cascade Förster resonance energy transfer (FRET) between NPs and NWs, which funnels the excitonic energy to the center of the superstructure invoking analogies with the process of photosynthesis. This effect has obvious importance for a variety of optoelectronic devices and energy conversion systems being currently investigated.

Experimental Section. CdTe NPs and NW with the stabilizer of thioglycolic acid were prepared as mentioned elsewhere in detail.[13,27] Streptavidin (SA) and D-biotin (B) were utilized to link two or three different nanomaterials. Biomolecules with inorganic nanomaterials were conjugated together by a standard EDC/sulfo-NHS procedure. Detailed procedures are described in previous publications.[21−23]

Three stock solutions of building blocks were prepared: dispersion of red-emitting CdTe NW with emission at 689 nm, orange-emitting NPs (NP_O) with emission at 582 nm, and green-emitting NPs (NP_G) with emission at 526 nm. NW was conjugated with B to reduce the possibility of precipitation after conjugation with biomolecules. NP_O were cross-linked with SA while NP_G were modified with B. After that the dispersions of NP_O−SA were added to the dispersion of NW−B spaced by a time interval sufficient for the formation of SA−B affinity pairs. The reaction of the formation of NP−NW complexes was followed by luminescence spectroscopy. Once the first step was completed NP_G−B dispersion was added and followed again by luminescence monitoring. The whole procedure was carried out in an optical quartz cuvette. Quantities of building block solutions (10−100 μL) were mixed together into 3 mL aliquots of deionized water (adjusted to pH 9 using 1 M NaOH solution). The photoluminescence (PL) spectrum was taken every 1−5 min for 1 h. When necessary, the conjugation reactions were carried out with only one size of NPs following the same procedure. The volume ratio of experiment was varied within 1−10 to obtain obvious spectral change of the FRET effect because the quantum yield of NW was generally quite lower than that of NPs that were used for the synthesis of NWs. All optical experiments were carried out with a Fluoromax-3 spectrofluorometer (Jobin Yvon/SPEX Horiba, NJ).

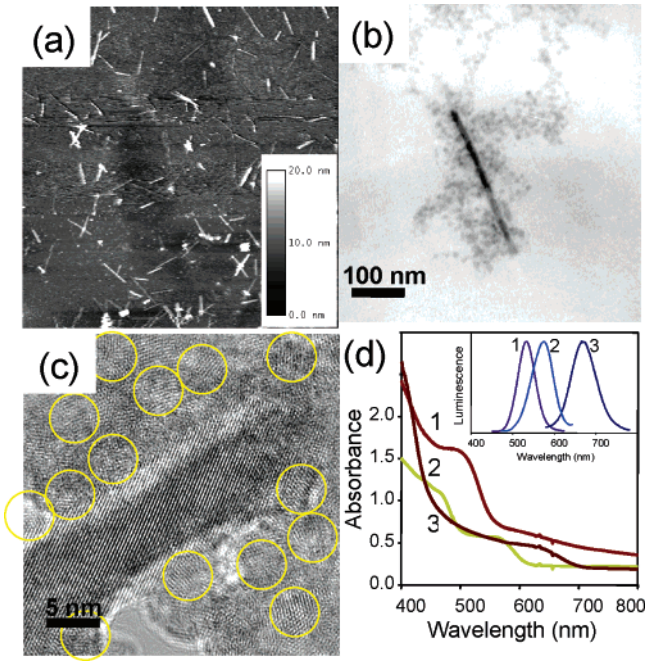

Figure 1. (a) AFM images of CdTe NWs (2.5 × 2.5 μm, the bar indicates the *z*-axis). (b, c) TEM images of NP conjugated NWs. Yellow circles in part c indicate CdTe NPs. (d) Absorbance and luminescence spectra of (1) NP_G, (2) NP_O, and (3) NW.

Results and Discussion. Cascade FRET was previously observed in NP thin films made by layer-by-layer assembly.[28,29] Very efficient transport of excitons from green-emitting NPs to red-emitting NPs could be seen initially empirically by Mamedov et al.[28] as substantial quenching of green luminescence in gradient films and later in formal study of FRET by Franztl et al.[29] When NPs are arranged according to their size in the stratified structures, both valence and conduction energy levels form a ramp. This property can be used in a variety of optoelectronic devices, for instance in light-emitting diodes, to reduce their turn-on voltage.[30−32] Considering that NWs represent an important basic element of nanoscale optoelectronic devices[21,33−36] and the same principles of charge transport should be applied to them as well, it would be interesting to create structures with similar functionalities. One-dimensional nanomaterials are ultimately suitable for transport of electrons and excitons, and therefore, creating an energy funnel with NW in its focus can open the door for many applications based on energy transfer.

Sequential attachment of a series of NPs to NW requires chemically active surfaces with chemical functionalities suitable for permanent bonding to NWs. CdTe NWs made by self-organization of stabilizer-depleted CdTe NPs offer this possibility.[13] The coatings made with thioglycolic acid with terminal COOH groups can be utilized for further derivatization by, for instance, biological entities.

Microscopy investigation by atomic force microscopy (AFM) and transmission electron microscopy (TEM) (Figure 1) indicates that the produced NWs were measured on

Table 1. Sizes and Emission Wavelengths of Synthesized NPs and NWs

	av size, nm	emission, nm	approx concn, M
NP green (NP_G)	3.2 ± 0.7	526	3.31×10^{-5}
NP orange (NP_O)	4.1 ± 1.2	582	1.57×10^{-5}
nanowires (NWs)		689	2.42×10^{-8}
diameter	6.62 ± 1.55		
length	512 ± 119		

average 6.62 ± 1.55 nm in diameter and 512 ± 119 nm in length (aspect ratio = 77). Only very few precursor particles could be seen in the NW dispersions. The NP → NW transition initiated by dipole−dipole attraction between the particles was virtually completed.

Physical sizes of NPs and proteins are comparable. For instance, considering that SA occupied by B has a hydrodynamic diameter of 5 nm,[37−40] there is a high likelihood of attachment of more than one SA unit to CdTe nanocrystals despite its size. Previously the presence of such conjugates was detected for CdTe−bovine serum albumin conjugates.[23] The same rationale could be applied to the attachment of the molecules of B to CdTe. Besides that, SA has four pockets for B docking. Therefore, the bioconjugates are inherently multivalent, which was demonstrated by producing networked agglomerates.[41−43] Optical and geometrical characteristics of NPs and NWs used here are listed in Table 1.

Sequential addition of NP building blocks to the NW dispersion as described in the Experimental Section results in fuzzy superstructures around the NWs as can be seen in a representative TEM images (Figure 1b). Many NPs are randomly linked on the surface of a NW (Figure 1b). Note that this image probably exaggerates the disorder on the NP "cloud" around the NW due to (1) distortions and possibly damages to the superstructure cause by drying and (2) the presence of unbound NPs forming a background image. In the high-resolution TEM image (Figure 1c), one can easily distinguish the borders of a NW and NPs. As expected, the NPs have a tendency to concentrate on and nearby the NW. The absorption and the PL emission spectra of the NWs and the two NPs indicate the possibility of the FRET in these superstructures, i.e., the effect from NPs to NW since one condition of the FRET effect is that the absorption spectrum of an acceptor must overlap the fluorescence emission spectrum of a donor because the Förster radius (R_o) is a function of spectral overlap integral ($J(\lambda)$).[44]

Initially, the energy transfer was realized between NW and NP_G superstructures (Figure 2). The wavelength of emission was 689 nm in NW−B and 526 nm in NP−SA. When NW and NP were conjugated in aqueous state, the PL change was immediately observed in both emission peaks with red shift of peak wavelength, as a gradually decreasing the PL intensity of NPs and increasing that of NWs, which is typical of the spectroscopic signature of the FRET. This process could be observed for an hour before reaching saturation. The time period of the reaction is very characteristic for the bioconjugation reactions and was similar for other systems involving NPs and NWs.[21,22,24]

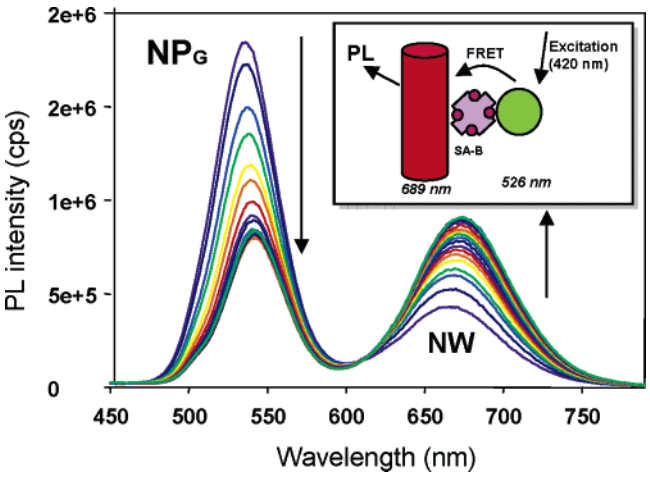

Figure 2. Typical experimental data of FRET effect on the bioconjugates between NPs and NWs. Arrows indicate the progression of spectra with time as bioconjugation reaction proceeds. The peak at 526 nm is decreasing while the peak at 689 nm is increasing, as the superstructure forms.

After that, a more complex superstructure was realized by sequential conjugation of NW and two different sizes of NPs, i.e., NW−B, NP_O−SA, and NP_G−B. If necessary, more layers can be created around the NW following the same approach. As can be seen from the emission wavelengths of nanocolloids used here (Table 1), the optical characteristics of superstructures made from particles of different diameters offer a possibility of a two-step FRET process: NP_G → NP_O → NW. Note that some degree of polydispersity of the NP is actually beneficial here because it removes the limitations related to most efficient overlap of excited energy levels in NPs.[45] Initially, the 100 μL of NW−B and 30 μL of NP_O−SA were mixed together, which yields the FRET spectra in Figure 3a−c (red arrows). The spectral evolution gave similarly clear indications of FRET here as in Figure 2 and previous studies.[24] After 21 min, 80 μL of the NP_G−B was added into this mixture. The mixture showed the spectral signature of energy transfer as well. As the PL intensity of NP_G and NP_O decreased, the PL intensity of NWs increased (Figure 3d,e, blue arrows). It is interesting to compare the two-step FRET superstructure with single-step energy transfer system. Under identical excitation conditions, the total PL intensity of NW in NW−NP_O−NP_G was enhanced two times when compared with NW−NP_O conjugate. Overall, 4-fold enhancement was observed in comparison with the original PL intensity of the free NW (Figure 3a) after addition of NP_G. This fact gives strong indication that indeed the cascade FRET process takes place resulting in the funneling excitons photogenerated in both NP_G and NP_O to the NW. It can be explained that the energy of NP_G is transferred to NP_O and then to NW through the NP_O when the entire superstructure is assembled in aqueous state (Figure 3, insert). Notice that the conjugation between NW and NP_G is not possible because both are used the same biological moieties, i.e., B, for conjugation.

Theoretical Model. It would be interesting to model the experimental data in Figures 2 and 3 related to the multistep energy transfer. As a start it is important to have an idea

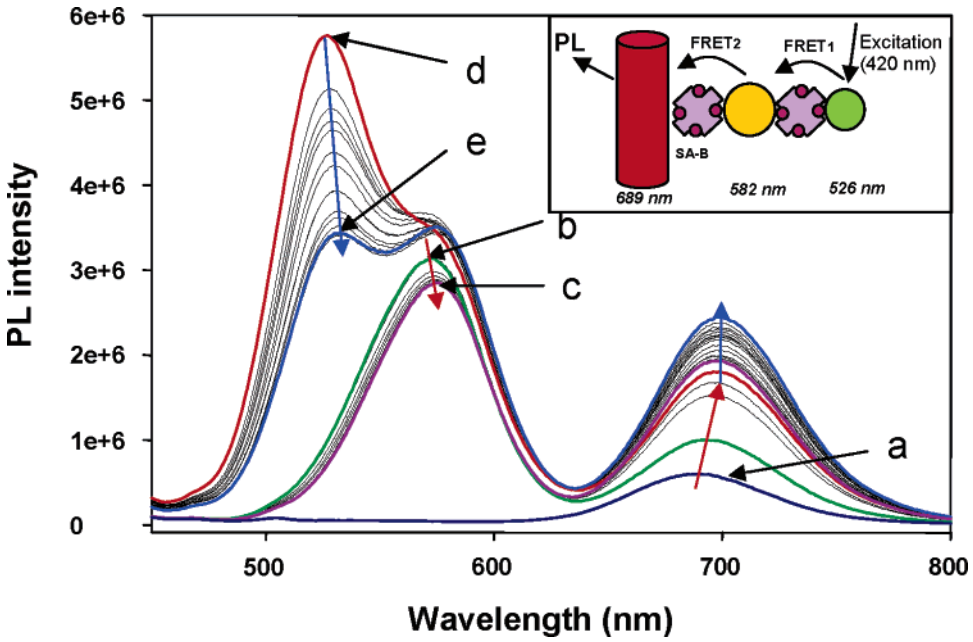

Figure 3. PL spectra of multiconjugated NW−NP superstructures: a, NW only; b, when NPO was added; c, after 21 min; d, when NPG was added; e, after 30 min (insert) schematic of the multiple conjugated NW−NP superstructures. Arrows indicate the progression of spectra with time as bioconjugation reactions proceeds. Red arrows correspond to the initial formation of NW−NPO conjugates. Blue arrows correspond to spectral changes started after addition of NPG to the formed NW−NPO assembly.

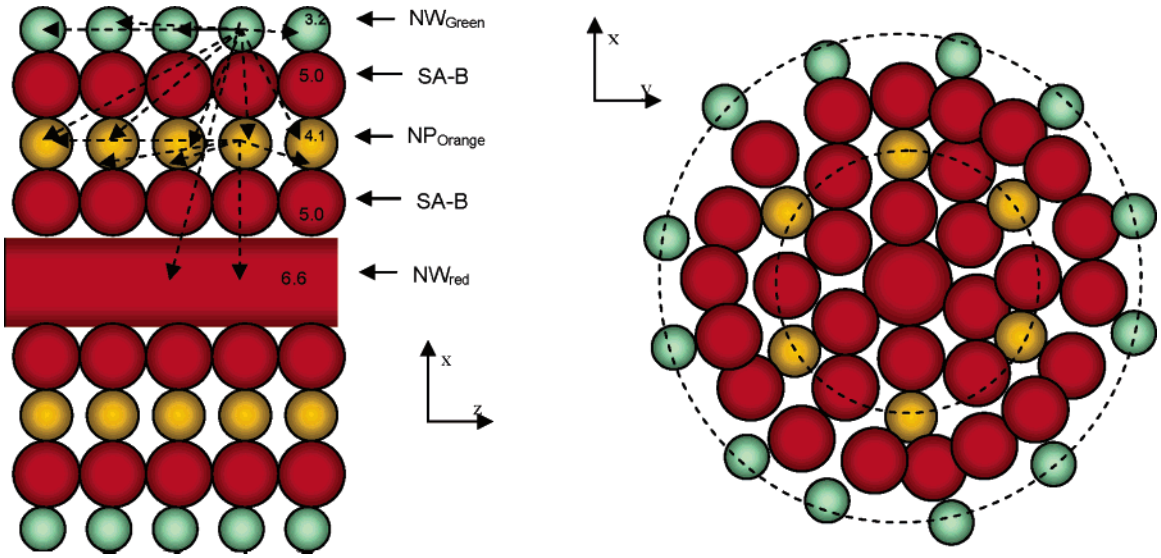

Figure 4. Theoretical model of the NW−NP superstructure. Left and right panels show cross sections of the structure in the $x-z$ and $x-y$ planes. The left panel also illustrates unidirectional Förster transfer from the smallest NP to other nanocrystals. The approximate radii of the shells of NPO and NPG are 10.35 and 19 nm, respectively.

about the stoichiometry of the produced assemblies. Evaluating the composition of the superstructure, we shall make the following assumptions: (1) complete transformation of Cd(2+) during the synthesis of NPs, (2) all NPs added to the solution of NWs become conjugated, and (3) one NP can carry more than one protein moiety. The first two of these assumptions are based on the experimental conditions use, i.e., the excess of the S(2−) and exceptionally high value of the streptavidin−biotin binding constant ($K_a = 10^{15}$ M $^{-1}$). The last assumption can be substantiated by the previous results for bovine serum albumin.[23,24] The average length of NWs was estimated from TEM images to be 512 nm. Under these conditions we arrive to the stoichiometric ratio of NPs and NWs: $m_{NPorange}/m_{NW} = 651$ and $m_{NPgreen}/m_{NW} = 1370$. Taking into account relative diameters of the assembly blocks, the structure of the assembly can be pictured by the schematics in Figure 4. It will consist of approximately 6 and 12 columns of NP_O and NP_G, respectively, attached to a single NW. The corresponding radii of the shells of NP_O and NP_G become 10 and 19 nm, respectively. For the SA−B linker size, we have chosen $d_{SA-B} = 5$ nm.

To model energy transport in this superstructure, we have to start from optical properties of individual NPs. The

important parameters of individual NPs are their exciton lifetimes ($\tau_\alpha = 1/\gamma_\alpha$) and quantum yields ($Y_\alpha$). Here γ_α denotes the rate of exciton recombination and the index α denotes a type of nanocrystal and can be NP_G, NP_O, or NW. The above parameters strongly depend on the particular realization and preparation of NPs and were measured as: $Y_{NP_G}, Y_{NP_O} \approx 10-20\%$, $Y_{NW} \approx 1-3\%$, $\gamma_{NP_G} \approx \gamma_{NP_O} \approx 1/18.8\ ns^{-1}$, and $Y_{NW} = 1/2.4\ ns^{-1}$. Note that here one needs to use the actual quantum yields and lifetimes of NPs and NWs in a fairly independent state, i.e., in solution. The effect of FRET, which results in apparent reduction of both parameters due to interaction with energy acceptors in the solid state will be taken into account in considering energy migration in the assembly. Additionally, strong reduction of quantum yield occurs in densely packed solids made of nanoparticles and other fluorophores. This is the case here (Figure 4) because particles are separated from each other by comparatively large molecules of proteins. The situation is analogous to conjugated polymers designed by the group of Swager,[50] which display luminescence as strong as in solution state, when a spacer that is added between fluorophores is added between polymeric chains.

In the simple rate model, the number of excitons (N_α) stored in a single NP is described by the dynamical equation: $dN_\alpha/dt = -\gamma_\alpha N_\alpha + I_\alpha$, where I_α is the intensity of light absorption in an α-type NP and t is the time. The recombination speed γ_α is composed of radiative and nonradiative rates: $\gamma_\alpha = \gamma_{\alpha,rad} + \gamma_{\alpha,nonrad}$. Under constant illumination, the time derivative in the rate equation is zero and the steady-state solution becomes equal to $N_\alpha = I_\alpha/\gamma_\alpha$. Then, we calculate the quantum yield of a nanocrystal: $\gamma_\alpha = \gamma_{\alpha,rad} N_\alpha / I_\alpha = \gamma_{\alpha,rad}/\gamma_\alpha$. In addition, we have to define the absorption rates of nanocrystals. As the simplest approach, we will assume that the absorption rate of a nanocrystal (I_α) is proportional to its volume. The whole emission spectrum of the NP_G-NP_O-NW system can be calculated as

$$I^{emiss}(\omega) = I^{emiss}_{NP_G} F(\omega - \omega_{NP_G}) + I^{emiss}_{NP_O} F(\omega - \omega_{NP_O}) + I^{emiss}_{NW} F(\omega - \omega_{NW}) \quad (1)$$

where I^{emiss}_α is the emission intensity of α-nanocrystals and $F(\omega) = \Gamma/[\pi(\omega^2 + \Gamma^2)]$ is the Lorentzian function and $\Gamma = 0.1$ eV. In eq 1, the emission intensities are given by $I^{emiss}_\alpha = m_\alpha N_\alpha \gamma_{\alpha,rad.}$

For Förster energy transfer, the exciton dynamics of individual NPs become strongly coupled in the superstructures. Due to fast energy relaxation inside individual NP or NW, this transfer occurs from NPs with larger band-gap to ones with smaller band-gap. The optical spectra in Figure 2 demonstrated transfer $NP_G \rightarrow NW$. In a more complex bioconjugate of Figure 3, we realized a transfer process: $NP_G \rightarrow NP_O \rightarrow NW$. The dynamics of interacting NPs and NWs is described by a system of coupled equations

$$\frac{dN_n}{dt} = -(\gamma_m + \sum_{m \neq n} \gamma^F_{n,m}) N_n + \sum_{m \neq n} \gamma^F_{m,n} N_m + I_\alpha \quad (2)$$

where N_m is the average number of excitons in a nanocrystal with number n and $\gamma^F_{m,n}$ is the rate of FRET from the m to n nanocrystal. In our model, we consider a complex made of a single NW and many NPs. Then, we number all NPs (NP_G and NP_O) and, for the NW, we adopt the index $n = 1$. Note that the transfer from m to n nanocrystals occurs only if the band-gap of m nanocrystal is larger or equal to the band-gap of n nano-object. For example, the transfer is possible from NP_G to all other NPs including neighboring NP_G, all NP_O, and the NW. At the same time, the FRET does not occur from the NW to NP_G and NP_O. Under constant illumination, the left-hand side of eq 2 is zero and we can easily solve the system of resultant linear equations using symmetry of the system: the numbers of excitons in NPs of the same kind are equal. We also assume that there is no net exciton transfer between NPs of the same kind since the populations of these NPs are the same. Provisions for and discussion of lateral exciton transfer in the shell along the NW axis are made below. Thus, we obtain

$$N_{NP_G} = \frac{I_{NP_G}}{(\gamma_{NP_G} + \gamma^F_{G\rightarrow O} I^{emiss}_\alpha)}$$

$$N_{NP_O} = \frac{I_{NP_O} + (m_{NP_G}/m_{NP_O}) N_{NP_G} \gamma^F_{G\rightarrow O}}{(\gamma_{NP_O} + \gamma^F_{O\rightarrow NW})}$$

$$N_{NW} = \frac{I_{NW} + (m_{NP_G}/m_{NW}) N_{NP_G} \gamma^F_{G\rightarrow NW} + (m_{NP_O}/m_{NW}) N_{NP_O} \gamma^F_{O\rightarrow NW}}{\gamma_{NW}} \quad (3)$$

where the parameters

$$\gamma^F_{G\rightarrow O} = \sum_{\text{from n-}NP_G\text{ to all }NP_O} \gamma^F_{n,m} \quad \text{and} \quad \gamma^F_{O\rightarrow NW} = \gamma^F_{NP_O,1}$$

determine inter-NP exciton transfer. Since the FRET rates rapidly decrease with interparticle distance,[42,43] and also for simplicity, we included only the sequential transfer processes $NP_G \rightarrow NP_O$ and $NP_O \rightarrow NW$. Therefore transfer $NP_G \rightarrow NP_{NW}$ is neglected since it is a relatively slow process.

First, we are going to consider the NP_G-NW complex (Figure 2). According to the molarities, the green NPs will form 12 columns and the characteristic distance between the NW center and the NP shell will be about 11.5 nm. The numbers of excitons in single NW and NP_G are given by equations similar to eq 3: $N_{NP_G} = I_{NP_G}/(\gamma_{NP_G} + \gamma^F_{n,1})$ and $N_{NW} = [I_{NW} + (m_{NP_G}/m_{NW}) N_{NP_G} \gamma^F_{G\rightarrow NW}]/\gamma_{NW}$. The emission spectrum of a NW−NP complex is composed of two peaks (526 and 689 nm) of intensities: $I^{emiss}_{NP_G} = m_{NP_G} \gamma_{rad,NP_G} N_{NP_G}$ and $I^{emiss}_{NW} = m_{NW} \gamma_{rad,NW} N_{NW}$. For the system just before conjugation, we obtain agreement between the experiment and theory taking reasonable numbers for the quantum yields as $Y_{NP_G} = 10\%$, $Y_{NW} = 3\%$. The calculated ratio between the peak intensities in Figure 5 before conjugation is about

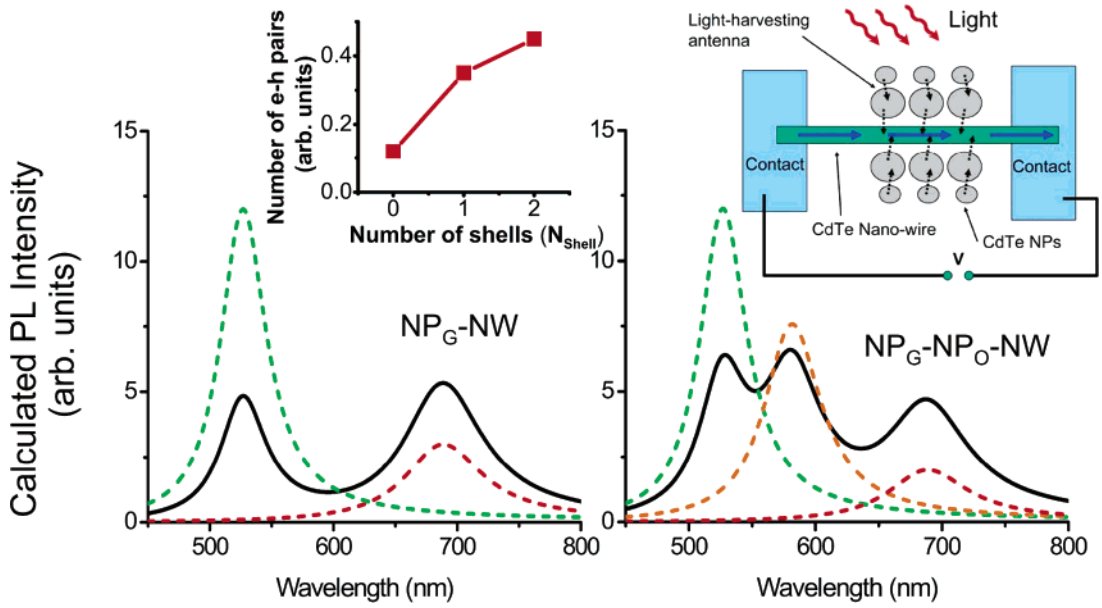

Figure 5. (left panel) Calculated emission intensity of the system of NW and NPG after conjugation for the parameters specified in the text (solid line). The dashed curves show the intensities of nonconjugated components. (right panel) Calculated emission intensity of the system of NW, NPO, and NPG after conjugation (solid line). The dashed curves show the intensities of nonconjugated components. (left insert) The peak intensity of NW as a function of the number of shells around a NW. Three data points correspond to the structures: NW, NPO−NW, and NPG−NPO−NW. (right insert) Schematic of suggested transport experiment involving a NP−NW complex and FRET. CdTe NPs absorb photons and transfer excitons toward the NW. Biological photosynthetic systems utilize a similar principle.

4, and the corresponding experimental ratio in Figure 2 is about 4.2. After conjugation, FRET strongly alters the emission spectrum. We can reproduce well the experimental spectrum after conjugation with $\gamma^{F}_{n,1} = \gamma^{F}_{NP_G,1} = 1/(12\ ns)$ (see Figure 5). The above rate corresponds to the transfer time 12 ns from NP_G to NW. It is interesting to compare FRET between two NPs and a NP and NW. In the first case, FRET couples two zero-dimensional systems and the distance dependence for the rate is usual: $\gamma^{F}_{NPnNP_m} \propto (\vec{R}_n - \vec{R}_m)^{-6}$. In the second case, FRET occurs between localized NP states and delocalized NW states. For exciton transfer from a zero-dimensional to one-dimensional system we obtain $\gamma^{F}_{NP_n} \propto R^{-5}$, where R is the distance between NP and NW. The dependence $\gamma^{F}_{NP_n} \propto R^{-5}$can be derived by integrating the Coulomb matrix element over delocalized wave functions of excitons in a NW.

To model a NP_G−NP_O−NW complex (Figure 4), we have to use eq 2. First, we have to pick up reasonable parameters for NP_O. For example, one can say that for NP of the same quality and structure $Y_{NP_G} > Y_{NP_O}$, which stems from the basic principles of quantum confinement. Indeed, we obtain agreement between theory and experiment for the spectra before conjugation by taking $Y_{NP_G} = 10\%$, $Y_{NP_O} = 6\%$, and $Y_{NW} = 2\%$. With the above numbers, the peak ratios in experimental and theoretical spectra coincide (see Figure 3e and Figure 4 right). Then, we can reproduce well the emission spectrum after conjugation (see Figure 3e and Figure 4 right) using the following parameters: $\gamma^{F}_{G\rightarrow O} = 1/(15\ ns)$ and $\gamma^{F}_{NP_O,1} = 1/(16\ ns)$. One can see that, in the conjugated complex, the emission peaks of NP_G and NP_O become reduced while the NW peak strongly grows. The FRET parameters obtained for the NP_G−NP_O−NW complex are not very different from those used for the NP_G−NW. This shows that the obtained rates of FRET provide us with reasonable estimates.

In our model a net "lateral" flow of excitons between NPs of the same size (i.e., the flow within one shell of the NP parallel to the NW axis) is equal to zero. This is true if all CdTe−NPs are of the same shape and diameter and have no defects. This approximation is convenient for theoretical consideration but has its limitations. We must admit that in real structures a small number of NPs may have strong structural defects and act as exciton drains or "black holes", which do not emit light at all. Exciton can flow to such "black holes" and recombine without photon emission. The theoretical model presented above will be valid if the distance between "black holes" in the NP corona is larger than the distance between NPs and NW. Assuming that the percentage of "black holes" in the population of NPs is small not exceeding, say a 1−2%, the distance that exciton needs to diffuse laterally to reach the "black hole" and sample 50−100 NPs is at least 150 nm (Figure 4), which greatly exceeds the distance between the layers. In fact, the system can possibly tolerate a much higher concentration of nonemitting NPs. As long as the probability of intershell exciton diffusion is larger than the probability of finding the "black hole", this model should give plausible data. Since it can describe well the experimental data, the above assumption is acceptable. One also needs to add that the lateral diffusion of excitons in NW is believed to be a very efficient process and is implicitly taken into account discussing the potential of this systems as energy funnels and optoelectronic devices. Comparing the lateral transport in NWs and NP shells, we also can see from the calculations that migration of excitons

along a NW leads to reduction of the total quantum yield of the system during conjugation. Before conjugation the averaged Y for the NP_G-NW complex is $Y^0_{NP_G-NW} \approx 6.5\%$, and after $Y^0_{NP_G-NW} \approx 4.3\%$.

If we consider the superstructure in Figure 4 as a light-harvesting device based on with directional FRET, photons become absorbed in NPs and then transferred to the NW. The photon energy of resulting emission becomes reduced (down converted). This suggests potential applications of NP−NW superstructures as optical nanodevices. To give a simple idea of how this effect could be utilized, a NW can be attached to the conducting leads for photocurrent measurements (Figure 5, insert). The conjugation of NW with NPs should result in the increased photocurrent responses since the NP subsystem leads to an increase of the number of photogenerated carriers inside the NW (Figure 5, insert). Note that the scheme of a NW-based device in Figure 5 qualitatively differs from the NW-based biosensors by other authors[46−49] where the attached molecules (such as DNA, for example) reduce the conductivity of NW due to the surface-depletion effect. In contrast, the attached NPs in our structure will increase the photocurrent.

Conclusions. In conclusion, we demonstrated a successful method to make the complex fuzzy superstructures of NPs and NWs with a degree of axial symmetry. The organization of the electronic properties of NPs in the shells allows for the multistep FRET from the external absorbing layer to the NW core. As a result of this process we see a 4-fold enhancement of light emission in the final NW energy acceptor compared with the nonconjugated state. This technique can be applicable for artificial energy harvesting photosynthetic processes, solar cells, and luminescence amplification devices and in nanoscale optoelectronic devices.

Acknowledgment. This work was supported by DARPA, NIH, NSF, and BNNT Initiative at Ohio University. The authors thank the reviewers for thoughtful comments.

References

(1) Koert, U.; Harding, M. M.; Lehn, J. M. *Nature* (*London*) **1990**, *346*, 339−342.
(2) Serroni, S.; Campagna, S.; Puntoriero, F.; Juris, A.; Denti, G.; Balzani, V.; Venturi, M.; Janzen, D.; Mann, K. R. *Inorg. Synth.* **2002**, *33*, 10−18.
(3) Ruben, M.; Rojo, J.; Romero-Salguero, F. J.; Uppadine, L. H.; Lehn, J. *Angew. Chem., Int. Ed. Engl.* **2004**, *43*, 3644−3662.
(4) Stadler, A. M.; Kyritsakas, N.; Lehn, J. M. *Chem. Commun.* **2004**, *18*, 2024−2025.
(5) Pina, F.; Passaniti, P.; Maestri, M.; Balzani, V.; Voegtle, F.; Gorka, M.; Lee, S. K.; Van Heyst, J.; Fakhrnabavi, H. *ChemPhysChem* **2004**, *5*, 473−480.
(6) Balzani, V.; Campagna, S.; Denti, G.; Juris, A.; Serroni, S.; Venturi, M. *Sol. Energy Mater. Sol. Cells* **1995**, *38*, 159−173.
(7) Dick, L. A.; Malfant, I.; Kuila, D.; Nebolsky, S.; Nocek, J. M.; Hoffman, B. M.; Ratner, M. A. *J. Am. Chem. Soc.* **1998**, *120*, 11401−11407.
(8) Benkoe, G.; Kallioinen, J.; Korppi-Tommola, J. E. I.; Yartsev, A. P.; Sundstroem, V. *J. Am. Chem. Soc.* **2002**, *124*, 489−493.
(9) Graetzel, M. *Coord. Chem. Rev.* **1991**, *111*, 167−174.
(10) Cherepy, N. J.; Smestad, G. P.; Graetzel, M.; Zhang, J. Z. *J. Phys. Chem. B* **1997**, *101*, 9342−9351.
(11) Wang, P.; Zakeeruddin, S. M.; Gratzel, M. *J. Fluorine Chem.* **2004**, *125*, 1241−1245.
(12) Gratzel, M. *Coord. Chem. Rev.* **1998**, *171*, 245−250.
(13) Tang, Z.; Kotov, N. A.; Giersig, M. *Science* **2002**, *297*, 237−240.
(14) Mokari, T.; Rothenberg, E.; Popov, I.; Costi, R.; Banin, U. *Science* **2004**, *304*, 1787−1790.
(15) Stevenson, K. A.; Muralidharan, G.; Maya, L.; Wells, J. C.; Barhen, J.; Thundat, T. *J Nanosci. Nanotechnol.* **2002**, *2*, 397−404.
(16) van Manen, H. J.; van Veggel, F. C. J. M.; Reinhoudt, D. N. *Top. Current Chem.* **2001**, *217*, 121−162.
(17) Ni, T.; Nagesha, D. K.; Robles, J.; Materer, N. F.; Mussig, S.; Kotov, N. A. *J. Am. Chem. Soc.* **2002**, *124*, 3980−3992.
(18) Ni, Tong, Nagesha, Dattatri K., Robles, Juvencio, Materer, Nicholas F., Mussig, Stefan, and Kotov, N. A. Unpublished results.
(19) Vayssieres, L. *Adv. Mater.* **2003**, *15*, 464−466.
(20) Hemker, K. J. *Science* **2004**, *304*, 221, 223.
(21) Wang, Y.; Tang, Z.; Tan, S.; Kotov, N. A. *Nano Lett.* **2005**, *5*, 243−248.
(22) Lee, J.; Govorov, A. O.; Dulka, J.; Kotov, N. A. *Nano Lett.* **2004**, *4*, 2323−2330.
(23) Mamedova, N. N.; Kotov, N. A.; Rogach, A. L.; Studer, J. *Nano Lett.* **2001**, *1*, 281−286.
(24) Wang, S.; Mamedova, N.; Kotov, N. A.; Chen, W.; Studer, J. *Nano Lett.* **2002**, *2*, 817−822.
(25) Decher, G. *Science* **1997**, *277*, 1232−1237.
(26) Kotov, N. A. *MRS Bull.* **2001**, *26*, 992−997.
(27) Gaponik, N.; Talapin, D. V.; Rogach, A. L.; Hoppe, K.; Shevchenko, E. V.; Kornowski, A.; Eychmueller, A.; Weller, H. *J. Phys. Chem. B* **2002**, *106*, 7177−7185.
(28) Mamedov, A. A.; Belov, A.; Giersig, M.; Mamedova, N. N.; Kotov, N. A. *J. Am. Chem. Soc.* **2001**, *123*, 7738−7739.
(29) Franzl, T.; Klar, T. A.; Schietinger, S.; Rogach, A. L.; Feldmann, J. *Nano Lett.* **2004**, *4*, 1599−1603.
(30) Schmidt-Mende, L.; Fechtenkotter, A.; Mullen, K.; Moons, E.; Friend, R. H.; MacKenzie, J. D. *Science 293*, 1119−1122.
(31) Berggren, M.; Dodabalapur, A.; Slusher, R. E.; Bao, Z. *Nature* (*London*) **1997**, *389*, 466−469.
(32) Tsang, W. T. *Appl. Phys. Lett.* **1981**, *39*, 134−137.
(33) Rosenthal, S. J.; Tomlinson, I.; Adkins, E. M.; Schroeter, S.; Adams, S.; Swafford, L.; McBride, J.; Wang, Y.; DeFelice, L. J.; Blakely, R. D. *J. Am. Chem. Society* **2002**, *124*, 4586−4594.
(34) Qian, F.; Li, Y.; Gradecak, S.; Wang, D.; Barrelet, C. J.; Lieber, C. M. *Nano Lett.* **2004**, *4*, 1975−1979.
(35) Zheng, G.; Lu, W.; Jin, S.; Lieber, C. M. *Adv. Mater.* **2004**, *16*, 1890−1893.
(36) Barrelet, C. J.; Greytak, A. B.; Lieber, C. M. *Nano Lett.* **2004**, *4*, 1981−1985.
(37) Yan, H.; Park, S. H.; Finkelstein, G.; Reif, J. H.; LaBean, T. H. *Science* **2003**, *301*, 1882−1884.
(38) Li, M.; Mann, S. *J. Mater. Chem.* **2004**, *14*, 2260−2263.
(39) Kaplan, D. L.; Davey, M. J.; O'Donnell, M. *J. Biol. Chem.* **2003**, *278*, 49171−49182.
(40) Shin, J. H.; Jiang, Y.; Grabowski, B.; Hurwitz, J.; Kelman, Z. *J. Biol. Chem.* **2003**, *278*, 49053−49062.
(41) Li, M.; Wong, K. K. W.; Mann, S. *Chem. Mater.* **1999**, *11*, 23−26.
(42) Li, M.; Mann, S. *J. Mater. Chem.* **2004**, *14*, 2260−2263.
(43) Li, M.; Schnablegger, H.; Mann, S. *Nature* (*London*) **1999**, *402*, 393−395.
(44) Foerster, T. *Ann. Phys.* **1948**, *2*, 55−75.
(45) Crooker, S. A.; Hollingsworth, J. A.; Tretiak, S.; Klimov, V. I. *Phys. Rev. Lett.* **2002**, *89*, 186802.
(46) Cui, Y.; Wei, Q.; Park, H.; Lieber, C. M. *Science* **2001**, *293*, 1289−1292.
(47) Besteman, K.; Lee, J. O.; Wiertz, F. G. M.; Heering, H. A.; Dekker: C. *Nano Lett.* **2003**, *3*, 727−730.
(48) Zhong, Z.; Wang, D.; Cui, Y.; Bockrath, M. W.; Lieber, C. M. *Science* **2003**, *302*, 1377−1380.
(49) Li, Z.; Chen, Y.; Li, X.; Kamins, T. I.; Nauka, K.; Williams, R. S. *Nano Lett.* **2004**, *4*, 245−247.
(50) McQuade, D. T.; Pullen, A. E.; Swager, T. M. Conjugated Polymer Sensory Materials. *Chem. Rev.* **2000**, *100*, 2537−2574.

NL051042U